# Nongeminate Recombination Dynamics–Device Voltage Relationship in Hybrid PbS Quantum Dot/C60 Solar Cells

*James W. Ryan,† Jose Manuel Marin-Beloqui,† Josep Albero,† and Emilio Palomares*,†,‡*

†Institute of Chemical Research of Catalonia (ICIQ), Avda. Països Catalans, 16, Tarragona. E-43007, Spain

‡ICREA, Passeig Lluís Companys 23, Barcelona E-08010, Spain

ABSTRACT: Here we employ transient optoelectronic techniques to study the charge present in the device and the nongeminate recombination rate in hybrid PbS/C60 planar heterojunction solar cells under working conditions. We find that in low light intensity conditions there are very few charges present in the solar cell and that the charge increases linearly with voltage, suggesting that most of the charge resides at the electrodes (capacitive charges). At higher applied light bias, the charges stored in the device increase exponentially. The carrier lifetime is very short (τ < 1 us at 1 sun; 1 sun = 100 mW/cm2 of sun-simulated light) when compared to organic solar cells. By correlating the charge carrier lifetime with the device charge density, we successfully reconstruct the photocurrent− voltage (J−V) curve at 1 sun, demonstrating that fast nongeminate recombination losses limit the efficiency in these quantum dot-based devices.

NTRODUCTION Organic solar cells (OSCs) are one of the most promising next generation photovoltaic technologies and have had their power conversion efficiency (PCE) improved significantly in recent years. More recently, inorganic colloidal quantum dots (CQDs) have also shown themselves to be promising candidates for next generation photovoltaics. Both approaches offer important characteristics for low-cost and high-throughput fabrication, such as low-temperature fabrication and compatibility with solution processing. However, with each approach there are limitations. A hybrid organic−inorganic approach is promising because it offers the possibility of maximizing the benefits of each material as well as minimizing the drawbacks and limitations of each respective compound. For example, OSCs have now exceeded power conversion efficiencies of 10% and are edging closer to the production line. However, some limitations still exist, with one being their inability to obtain a very high photocurrent because of their intrinsic low exciton diffusion lengths. Furthermore, it is difficult to have efficient organic semiconductors that can extend their absorption far into the near-infrared (NIR), which limits their ability to cover the entire spectrum. However, colloidal quantum dot (CQD) based solar cells can extend their absorption further into the NIR with PbS or PbSe nanocrystals and have recently shown high efficiencies exceeding 7%.1,2 CQDs have several advantages over organic semiconductors, such as their

optical properties, the ability to have their absorption characteristics tuned simply by changing the nanocrystal size,3,4 and the capability of multiple-exciton generation.5 Another advantage is that they have higher dielectric constants, meaning that, in comparison to organic semiconductors, they allow spontaneous generation of free charge carriers under light irradiation. Several approaches utilizing quantum dots have already been demonstrated in the literature, such as Schottky devices,6 depleted heterojunctions,7 quantum dot sensitized solar cells (QDSSC),8 and bulk heterojunction (BHJ) QD:polymer9 and bilayer CQD/small molecule solar cells.10 Pb-based nanocrystals have shown the best device efficiencies because of the their excellent optical properties in that they possess the characteristic of being panchromatic with the ability to extend their absorption into the infrared by increasing their diameter,4,11 allowing a larger portion of the solar spectrum to be harvested compared to that captured by Cd-based CQDs; this leads to devices with extremely high photocurrents.2

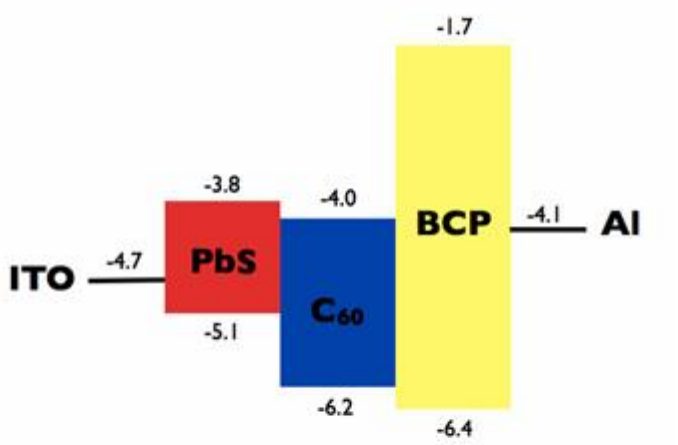


**Figure 1.** Energy levels for the materials used in these devices PbS (15 nm)/C60(40 nm)/BCP(10 nm)/Al(100 nm).

However, the further one wishes to extend the absorption of the CQDs into the NIR, the lower the band gap becomes, which in turn affects the open circuit voltage (VOC).12 The device architecture can also limit the VOC; for example, the maximum achievable VOC for a Schottky or depleted heterojunction device is limited by the work functions of the electrodes. A method to decouple the influence of the contacts on the VOC is to employ a donor−acceptor type-II heterojunction in which the VOC is instead determined by the difference between the donor HOMO (valence band) and the acceptor LUMO (conduction band) of the organic (inorganic) semiconductors. The VOC is simply the point at which no net current flows in a device, where the flux of charge generation is equal to the flux of charge recombination. PbS CQD devices have also used this heterojunction approach with PbS acting as the donor and a metal oxide (ZnO),13 a CQD (Bi2S3),14 or an organic component (C60)10 acting as the acceptor. Hybrid inorganic CQD/organic devices are particularly interesting, especially considering the difficulty in

designing efficient NIR chromophores that can absorb at wavelengths beyond 800 nm. Using CQDs with organic semiconductors offers exciting prospects for single-junction solar cells with absorption extending into the NIR much further than is possible using a pure organic active layer. Furthermore, this approach also opens the door to tandem solar cells. Previously, we have studied the charge transfer kinetics and nongeminate charge recombination dynamics for a number of QDSSC and QD:polymer solar cells through the use of transient optical and optoelectronic techniques,15–18 and we now extend the analysis to bilayer PbS quantum dot/C60 devices to quantify the rate of nongeminate recombination with respect to the charge density in the device and use this information to understand the impact nongeminate recombi nation has on the VOC in these devices. An added advantage of choosing a bilayer architecture is that we can control the interface instead of having a disordered BHJ morphology that is common for QD:polymer devices.

## Experimental Section

**Semiconductor Nanocrystal Synthesis**. PbS CQDs were prepared following a slightly modified procedure described by Sargent et al.33 35 mL of 1-octadecene (ODA) was heated at 80 °C under vacuum for 9 h. Then 0.45 g of PbO, 1.3 mL of oleic acid, and 3 mL of distilled ODE were placed under vacuum for 16 h at 95 °C. The color of the solution changed from yellow to transparent, and 15 mL of degassed ODE was added; the temperature was raised to 120 °C, and a degassed solution of 210 μL of bis(trimethylsilyl)sulphide (TMS) in 10 mL of ODE was steadily injected. The solution was then allowed to cool to room temperature. The solution was precipitated with acetone and redispersed in toluene to remove the reaction side products. The dried product was then dispersed in 3 mL of toluene, and 1 mL of distilled oleyamine was added. This solution was stored in a glove box under a N2 atmosphere for two days without disruption. The CQD solution was then precipitated with methanol and redispersed in toluene three times. Finally, the CQDs were dispersed in anhydrous octane at a concentration of 10 mg/mL. The average QD size was 3 nm.

**Device Preparation and Characterization.** Devices were fabricated with the following structure: ITO / PbS (15 nm) / C60 (40 nm) / BCP (8 nm) / Al (100 nm). First, indium tin oxide (ITO, Psiotech Ltd., 5 Ω/square) substrates were cleaned by three sonication cycles. The first was in acetone, and the two following cycles were in isopropanol; each cycle lasted 15 min. Then the substrates were subjected to 20 min of UV/O3 treatment. PbS CQD films were grown using a layer-by-layer spin-coating procedure with a 10 mg/mL PbS CQD solution that included a ligand exchange process after deposition of each layer whereby the bulky oleyamine and oleic acid ligands were replaced by 3-mercaptopropionic acid (MPA) by spin coating a solution of MPA dissolved in methanol (10% v/v). After each ligand exchange step, excess ligands and QDs were rinsed from the

films using methanol and octane, respectively. Finally, the substrate was briefly annealed at 470 °C through the use of a heat gun; then the next PbS layer was ready to be deposited. Each layer corresponded to approximately 2 monolayers (5 nm). Devices consisted of a total of 3 layers, producing films with a thickness of 15 nm as measured by transmission electron microscopy. The films were transferred to a high-vacuum chamber where C60 (40 nm), BCP (8 nm), and Al (100 nm) were deposited by thermal evaporation at a base pressure not exceeding 1 × 10−6 mbar. Devices were measured in the dark and under AM 1.5G conditions using an Abet Solar 2000 solar simulator and a Keithley 2400 digital source meter to apply bias and record the current. A Labview interface was used to control the source meter and record the I−V curves. A calibrated silicon diode (NREL) was used to obtain 1 sun conditions, and lower light conditions were simulated using neutral density filters. All devices were measured in a sealed holder under a N2 atmosphere. The measurement of incident photon-to-current conversion efficiency (IPCE) was plotted as a function of the excitation wavelength using the incident light from a 300 W xenon lamp (ILC Technology), which was focused through a Gemini-180 double monochromator (Jobin Yvon Ltd.) For transient photovoltage (TPV) measurements, the devices were connected to the 1 MΩ input terminal of an oscilloscope and illuminated with white light to set the light bias. A small optical perturbation was applied using a nitrogen-pumped PTI GL-301 dye laser as the excitation source at a wavelength of 470 nm (frequency, 1.5 Hz; pulse duration by three sonication cycles. The first was in acetone, and the two following cycles were in isopropanol; each cycle lasted 15 min. Then the substrates were subjected to 20 min of UV/O3 treatment. PbS CQD films were grown using a layer-by-layer spin-coating procedure with a 10 mg/mL PbS CQD solution that included a ligand exchange process after deposition of each layer whereby the bulky oleyamine and oleic acid ligands were replaced by 3-mercaptopropionic acid (MPA) by spin coating a solution of MPA dissolved in methanol (10% v/v). After each ligand exchange step, excess ligands and QDs were rinsed from the films using methanol and octane, respectively. Finally, the substrate was briefly annealed at 470 °C through the use of a heat gun; then the next PbS layer was ready to be deposited. Each layer corresponded to approximately 2 monolayers (5 nm). Devices consisted of a total of 3 layers, producing films with a thickness of 15 nm as measured by transmission electron microscopy. The films were transferred to a high-vacuum chamber where C60 (40 nm), BCP (8 nm), and Al (100 nm) were deposited by thermal evaporation at a base pressure not exceeding 1 × 10−6 mbar. Devices were measured in the dark and under AM 1.5G conditions using an Abet Solar 2000 solar simulator and a Keithley 2400 digital source meter to apply bias and record the current. A Labview interface was used to control the source meter and record the I−V curves. A calibrated silicon diode (NREL) was used to obtain 1 sun conditions, and lower light conditions were simulated using neutral density filters. All devices were measured in a sealed holder under a N2 atmosphere. The measurement of incident photon-to-current conversion efficiency (IPCE) was plotted as a function of the excitation wavelength using the incident light from a 300 W xenon lamp (ILC Technology), which was focused through

a Gemini-180 double monochromator (Jobin Yvon Ltd.) For transient photovoltage (TPV) measurements, the devices were connected to the 1 MΩ input terminal of an oscilloscope and illuminated with white light to set the light bias. A small optical perturbation was applied using a nitrogen-pumped PTI GL-301 dye laser as the excitation source at a wavelength of 470 nm (frequency, 1.5 Hz; pulse duration working conditions using a home-built system. Devices were held at open circuit by applying bias from either a focused array of LEDs or an external power source (Keithley 2400 digital source meter). In the case of a bias applied from a power source, the devices were still subject to illumination. Once the device reached steady state, it was then short-circuited and the LEDs were switched off simultaneously (switch-off time/relay = 300 ns), leaving the charge stored in the active layer to decay through a small 50 Ω resistor. A Yokogawa 2052 digital oscilloscope was used to record the voltage decay across the resistor. Using Ohm's law, the voltage transient could be turned into a current transient. This was subsequently integrated to calculate the total charge in the active layer at circuit voltage values ranging from the voltage corresponding to >1 sun conditions to 0 V (or extending into the negative when required). In some instances the lifetime of the voltage transient and the nongeminate recombination rate are of the same order. Therefore, we use an iterative procedure using a home-built MatLab program to calculate the incurred charge losses during extraction.

## RESULTS AND DISCUSSION

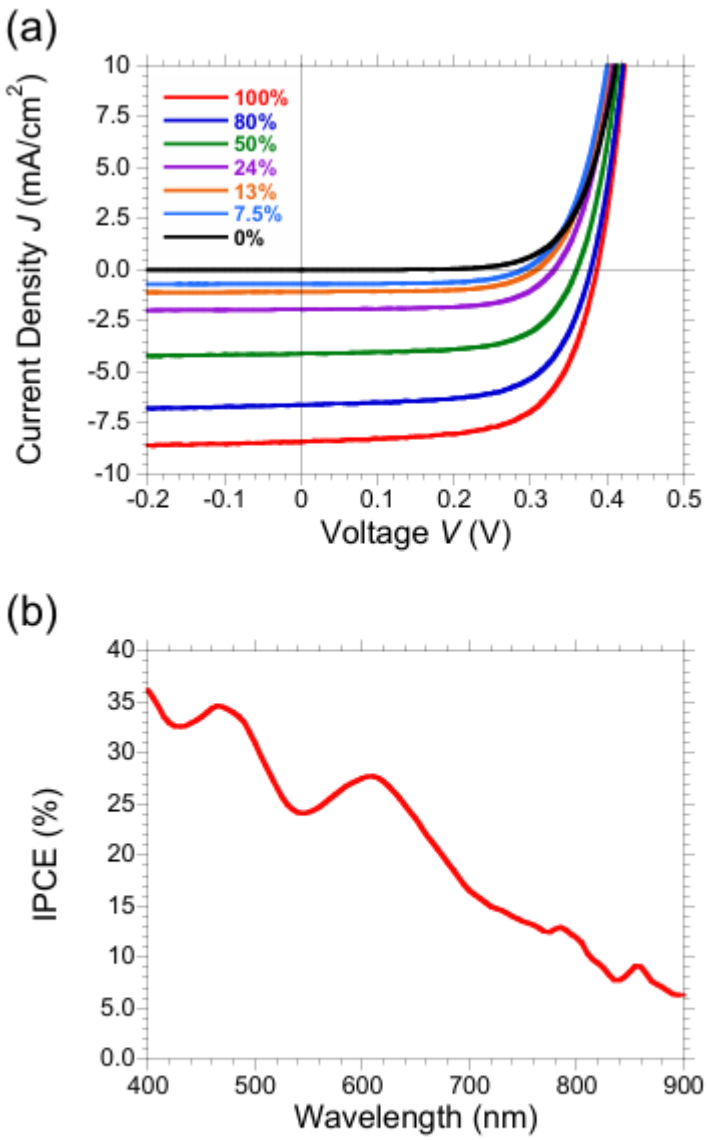


**Figure 2.** Current/voltage curves (a) for devices measured under standard AM 1.5 G conditions (100 mW/cm2), where the intensity of irradiance was fixed using neutral density filters. The legend shows the % of irradiance with respect to 1 Sun illumination, calculated using a calibrated silicon diode. IPCE for the corresponding device is shown in (b).

We employ transient optoelectronic techniques, namely charge extraction (CE) and transient photovoltage (TPV), to quantify the charge density and nongeminate recombination rate of PbS/C60 planar heterojunction solar cells under working conditions. (Device architecture and typical energy levels of the materials are shown in Figure 1, while device fabrication and PbS CQD synthesis are described in Experimental Section.) Correlating the charges present in the device with the charge carrier lifetime allows us to accurately reconstruct the experimental current−voltage curve using the model introduced for organic solar cells.19 To the best of our knowledge, this is the first time it has been reported for hybrid organic−inorganic solar cells based on CQDs. The current−voltage (J−V) curves of the device under various light intensities measured using a calibrated solar simulator (AM 1.5 G, 100 mW/cm2) are shown in Figure 2a. The device

shows a short circuit current, JSC, of 8.26 mA/cm2,a VOC of 0.38 V, and a fill factor (FF) of 0.64, corresponding to a power conversion efficiency of η = 2.04% at 1 sun. Figure 3a shows the relationship between JSC and light intensity (LI), which has a power law behavior with the relationship $P \propto LI^{\alpha}$, with α = 1.01, which signifies that nongeminate recombination at short circuit is negligible and that there is no significant space charge buildup.20,21 The correlation between VOC and LI is also shown in Figure 3b, showing a linear increase of VOC with the logarithm of LI. The slope of the curve in an ideal diode would correspond to the thermal voltage kBT, the deviation from ideal behavior is termed the ideality factor and is calculated from the following equation:

$$n_{\mathrm{id}} = \frac{e}{k_{\mathrm{B}}T}\frac{\mathrm{d}V_{\mathrm{OC}}}{\mathrm{d}\ln(\mathrm{LI})} \quad (1)$$

where e is the elementary charge and kBT is the thermal energy, with nid = 1.47. Generally, the ideality factor ranges from 1 to 2, and it provides information on the origin of the charge recombination that occurs in a device. An ideality factor increasing from 1 indicates the presence of trap states, with higher values corresponding to the presence of deeper and more abundant traps. The ideality factor also gives an indication of what process is determining the charge carrier recombination dynamics; nid = 1 signifies bimolecular recombination, and nid = 2 indicates Shockley–Read–Hall (SRH) recombination.12,22 Therefore, the rather high ideality factor obtained for PbS/C60 suggests that there is a significant concentration of trap states, which will affect the nongeminate recombination dynamics. In related studies, trap states (midgap states) have been shown to affect nongeminate recombination and the VOC in PbS/methano-fullerene bilayers, although no relationship with charge carrier density was shown.23 To quantify the charge present in the device under illumination, we employed the charge extraction technique, as used in previous publications by our group and others.24,25 For this experiment, the device is held at open circuit by applying either a light or electrical bias through a set of LEDs or external power source until the steady state is reached (1−2 s) and then switched from open circuit to short circuit while simultaneously switching off the LEDs. Sweeping the bias from values higher than VOC at 1 sun (VOC = 0.38 V at 1 sun in this case) to dark conditions allows a good estimate of the charge present in the device under working conditions. Figure 4 shows the charge density plotted versus applied bias. For the standard CE measurement, where bias is applied from a set of LEDs, we found that at low applied bias the charge density shows a linear dependence on applied bias.

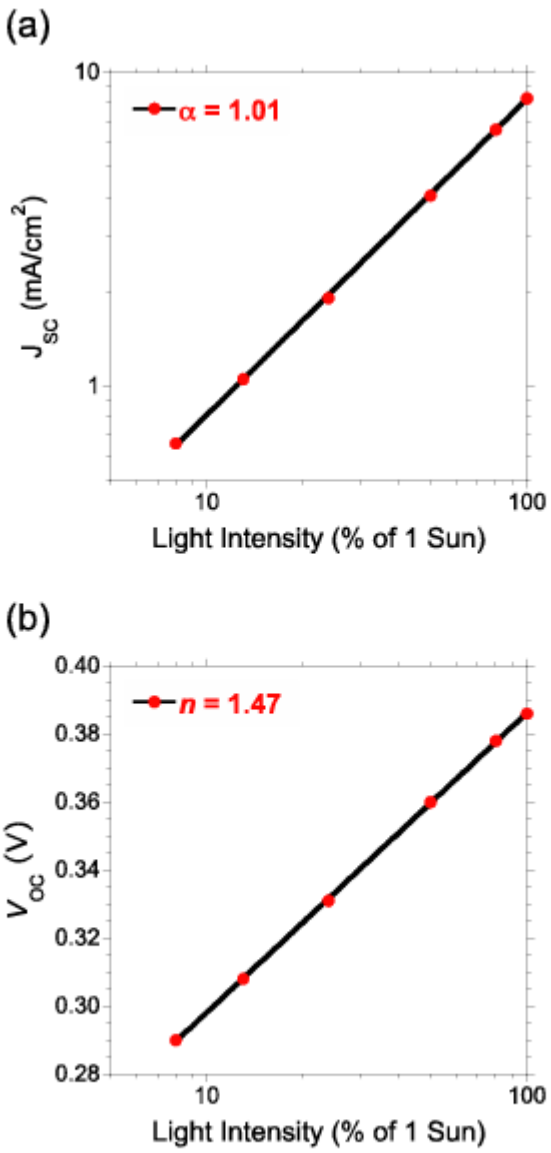


**Figure 3.** $J_{SC}$ (a) and $V_{OC}$ (b) plotted versus light intensity. In (a) α corresponds to the power law fit where $P \propto LI^{\alpha}$ and in (b) n corresponds to the ideality factor obtained from Equation (1).

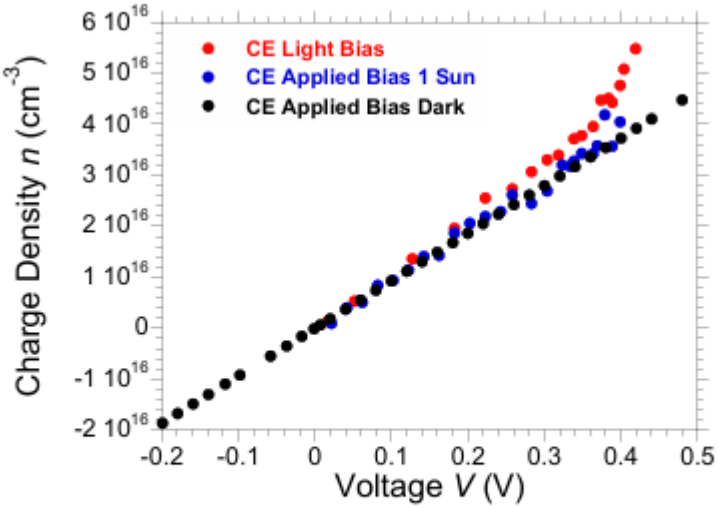


**Figure 4.** Photo-nduced charge extraction data for the same device measured under light bias and applied bias (dark and 1 Sun illumination). Charge losses during extraction are accounted for.

However, when the applied bias increases sufficiently, the charge density shows an exponential dependence on applied bias. The linear dependence of charge versus bias at low light intensity was found to be a result of the geometrical charges, obtained by carrying out CE measure ments in the dark and under negative bias, as reported previously,20 and was found to be 83 nF/cm2. This signifies that there is very little chemical charge built up in the active layer at low light bias; the charges are mostly present at the electrodes. At increased forward bias, the charges in the device begin to increase exponentially to values higher than the corresponding capacitive charges. The charges can therefore be related to excess charge carriers generated in the photoactive region. This exponential increase has been previously attributed to the splitting of the quasi-Fermi levels in donor and acceptor molecules in organic bulk-heterojunction solar cells.19 We can f it the data in Figure 2 according to the following equation that n ne V oc correlates the charges in the device with the VOC:

$$n = n_0 e^{\gamma V_{oc}} \quad (2)$$

where, n0 ~ 2.77 × 1015 carriers/cm3 and γ ~ 7.12 V−1, ifwe consider the total charge in the device. (2) The parameter γ provides an estimate of the tail of the density of states (DOS) and is considerably lower than an ideal semiconductor (γ< 19V−1 for 2kT). This points toward the system having a high density of trap states and is consistent with the ideality factor measured from Figure 3b.26 Our observations here of a low number of carriers and a low γ are similar to previous charge extraction measurements of planar heterojunction solar cells20,25,27 and are due to the thin nature of the films and high energetic disorder.19,28 TPV measurements provide a measurement of the charge

carrier lifetimes in the device. The TPV experiment consists of holding the device at open circuit under steady state conditions by applying a light bias via a ring of LEDs, akin to the CE measurements. Next, a small perturbation is applied to the device; in this case, the perturbation is applied by a laser. The small perturbation (5–10 mV) generates extra charges in the device that cannot be extracted because the system is being held at open-circuit, forcing the charges to recombine. An added advantage of this technique is that the small excess charge generated decays monoexponentially, making it easy to calculate the excess charge carrier lifetime:

$$\Delta n = \Delta n_0 e^{-t/\tau_{\Delta n}} \quad (3)$$

where t is the time, Δn0 the photogenerated charge at t = 0, and τΔn the lifetime of the transient. For each point on the current– voltage curve we can obtain a specific lifetime. A plot of the measured small perturbation lifetimes, τΔn, as a function of VOC is shown in Figure 5, which shows a nonlinear relationship between charge carrier lifetime and applied bias. In fact, the charge carriers decay exponentially with bias according to the function

$$\tau_{\Delta n} = \tau_{\Delta n_0} e^{-\beta V_{OC}} \quad (4)$$

where τΔn0 is ∼0.012 s and the decay constant β is ∼24.94 V−1. This exponential decay is consistent with the behavior of organic solar cells. At 1 sun conditions, τΔn is< 1 μs; these lifetimes are very short in comparison to those of higher VOC OSCs, which already suggests the reason for the low device VOC. Having now obtained the relationship between τΔn and applied bias as well as the behavior of n with applied bias, we can correlate τΔn with n by interpolating the applied bias with the exponential fit obtained from CE under light bias. Figure 6 shows the lifetime versus charge density, which displays a power law behavior

$$\tau_{\Delta n} \propto n^{-\lambda} \quad (5)$$

The power law, λ, can also be calculated simply by considering the exponential decay of τΔn versus bias (β) and the exponential growth of charge density versus bias (γ): β/γ = λ. However, the parameter λ relates the charge density with the small perturbation charge carrier lifetime, as opposed to the total charge carrier lifetime, τn. Correcting for this is rather simple and has been shown to apply to both OSCs and dye sensitized solar cells, with the total charge carrier lifetime

$$\tau_n = \tau_{\Delta n}(\lambda + 1) \quad (6)$$

It has been shown for organic solar cells that the relationship between n and τn gives the empirical reaction order, Φ (Φ = λ + 1) of the free charge carriers, with some values suggesting bimolecular recombination.19,29,30 For the measured PbS/C60 devices here, we obtain an empirical reaction order of 3.5. This value is too high for what we would expect for bimolecular recombination, but is not uncommon for such a thin active layer.

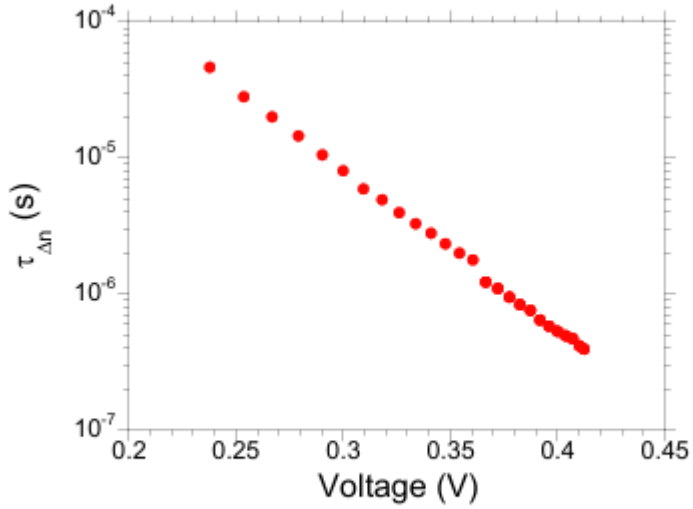


**Figure 5.** Small perturbation lifetime *versus* lifetime obtained from PIT-PV measurements.

For OSCs, many devices have also shown high reaction orders, especially when the active layer is very thin.31,32 One of the reasons for the high Φ values is a large gradient in carrier concentration31 due to energetic disorder, surface recombina tion, and trap-assisted recombination. What is important here, however, is that the relationship still gives us accurate information on the rate at which the charges are recombining within the device even though the origin of the recombination is not clear. It is most likely a convolution of different events occurring at the PbS/C60 interface, within each respective layer, or at the contacts. Having determined the correlation between charge density and charge carrier lifetime in the active layer, we attempt to reconstruct the J–V behavior of the hybrid PbS/C60 device under 1 sun conditions. Durrant and co-workers have shown that a simple model that takes into account the flux of photogenerated charges (Jgen) and the flux of nongeminate recombination (Jloss) makes it is possible to reconstruct the J–V curve accurately32 using the relationships

$$J = J_{gen} + J_{loss}$$

$$J_{loss} = \frac{edn}{\tau_n} \quad \text{(7)and (8)}$$

where d is the thickness of the active layer, n the charge density, and τn the charge lifetime. In this approximation, it is assumed that the loss processes are simply due to nongeminate recombination and are negligible close to short-circuit. When the bias is increased closer to VOC, the nongeminate recombination begins to increase significantly, and at VOC the f lux of nongeminate recombination equals that of Jgen.

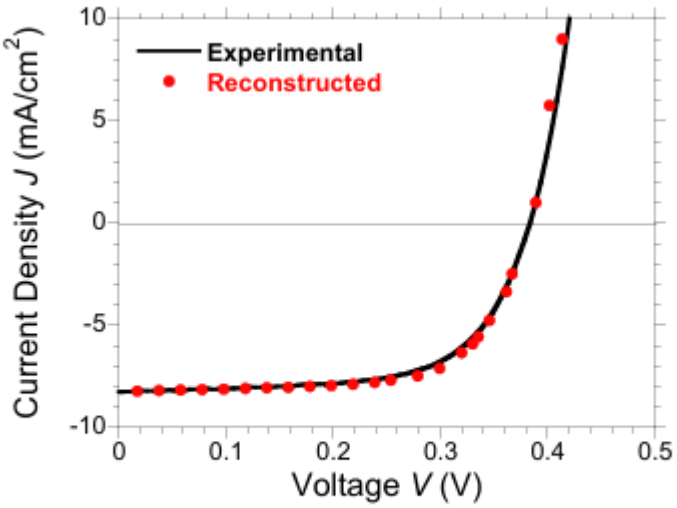


**Figure 7.** Comparison between the reconstructed *JV* curve using Equation 7 and the experimental *JV* curve as presented in **Figure 2**.

Carrying out CE under 1 sun illumination conditions (Figure 4) and applied electrical bias allows n to be calculated for each point across the J–V curve. To reconstruct the J–V curve with the experimental curve shown for 1 sun in Figure 2, we allow Jgen = JSC and calculate Jloss using eq 8. An additional correction to account for the small photoshunt is also applied using the experimental J–V data. This correction does not affect the calculated VOC we obtain, and any nongeminate recombination causing it can be ruled out based on the relationship between JSC and LI (power law with α = 1.01; see Figure 3a). We correct for the voltage in the cell by considering Vcell = Vappl − IRs, where Rs is the series resistance. The experimental and reconstructed J–V curves are shown in Figure 7 and are in good agreement, with the reconstructed VOC exactly matching the experimental VOC (0.383 mV). In other similar devices that we measured there was a small fluctuation between the calculated VOC and the experimental VOC, consistent with the trend observed for a range of different organic solar cells.32 The fact that the 1 sun J–V behavior can be reproduced using this simple relationship between generation and recombination signifies that the origin the VOC in these devices is field independent and is controlled by

nongeminate recombination. Knowing that nongeminate recombination is the key loss mechanism affecting the VOC thus provides a route toward further optimization of device performance. Reducing the concentration of trap states is perhaps the most significant step for optimization. CQDs in particular tend to have a high distribution of midgap states that trap charges and thus push the ideality factor higher; reducing these trap states will reult in more ideal diode behavior, longer charge carrier lifetime, and thus higher VOC. Recently, CQD solar cells have seen improvements in VOC with either a reduction in trap states or through doping the transition metal acceptor. It will be interesting to see if the same procedure used to reconstruct the J–V curve can be applied to other CQD-based solar cells such as depleted heterojunction devices that have a different working mechanism but, similar to organic semiconductors, tend to have a high degree of energetic disorder unlike their bulk materials.

## CONCLUSIONS

In summary, we have studied the optoelectronic performance of PbS/C60 devices through both steady state J–V character ization and transient optoelectronic measurements. From the data obtained, we see that the open circuit voltage increases linearly with the logarithm of LI, which is evidence for the increased splitting of quasi-Fermi levels with LI. We correlated the relationship to obtain an ideality factor of 1.47, indicating quite a large density of traps that affect nongeminate recombination. Furthermore, on the basis of the relationship between JSC and LI, nongeminate recombination is negligible at short circuit, suggesting that the origin of the photoshunt is a f ield-dependent generation process. The charge carrier lifetime in the films is short, on the order of 1 × 10−6 s, with a steep decay order of 24.94, meaning charge carrier lifetime decreases rapidly with increasing bias. The charge density in the active layer is very low, as seen for similar organic bilayer devices, with most of the charges residing at the electrodes under low-bias conditions, and increases exponentially close to VOC. Using the relationship between Jgen and Jloss, we could accurately reconstruct the J–V curve, proving that here VOC is field independent and can be improved by reducing the rate of nongeminate recombination. More important, our results clearly demonstrate that increasing the lifetime of the charge carriers through reducing the trap states present at the PbS/C60 interface will lead to higher VOC and improved efficiencies. Thus, the greatest potential for improvement lies with the PbS CQD synthesis and choice of the ligands/passivation layer.

## References

(1) Kramer, I. J.; Sargent, E. H. Colloidal QuantumDot Photovoltaics: A Path Forward. ACS Nano 2011, 5, 8506−8514. (2) Ip, A. H.; Thon, S. M.; Hoogland, S.; Voznyy, O.; Zhitomirsky, D.; Debnath, R.; Levina, L.; Rollny, L. R.; Carey, G. H.; Fischer, A.; Kemp, K. W.; Kramer, I. J.; Ning, Z.; Labelle, A. J.; Chou, K. W.; Amassian, A.; Sargent, E. H. Hybrid Passivated Colloidal Quantum Dot Solids. Nat. Nanotechnol. 2012, 7, 577−582. (3) Alivisatos, A. P.

Semiconductor Clusters, Nanocrystals, and Quantum Dots. Science 1996, 271, 933–937. (4) Moreels, I.; Lambert, K.; Smeets, D.; De Muynck, D.; Nollet, T.; Martins, J. C.; Vanhaecke, F.; Vantomme, A.; Delerue, C.; Allan, G.; Hens, Z. Size-Dependent Optical Properties of Colloidal PbS Quantum Dots. ACS Nano 2009, 3, 3023–3030. (5) Semonin, O. E.; Luther, J. M.; Choi, S.; Chen, H.-Y.; Gao, J.; Nozik, A. J.; Beard, M. C. Peak External Photocurrent Quantum Efficiency Exceeding 100% via MEG in a Quantum Dot Solar Cell. Science 2011, 334, 1530–1533. (6) Tang, J.; Wang, X.; Brzozowski, L.; Barkhouse, D. A. R.; Debnath, R.; Levina, L.; Sargent, E. H. Schottky Quantum Dot Solar Cells Stable in Air under Solar Illumination. Adv. Mater. 2010, 22, 1398–1402. (7) Pattantyus-Abraham, A. G.; Kramer, I. J.; Barkhouse, A. R.; Wang, X.; Konstantatos, G.; Debnath, R.; Levina, L.; Raabe, I.; Nazeeruddin, M. K.; Graetzel, M.; Sargent, E. H. Depleted-Heterojunction Colloidal Quantum Dot Solar Cells. ACS Nano 2010, 4, 3374–3380. (8) Santra, P. K.; Nair, P. V.; Thomas, K. G.; Kamat, P. V. CuInS2 Sensitized Quantum Dot Solar Cell. Electrophoretic Deposition, Excited-State Dynamics, and Photovoltaic Performance. J. Phys. Chem. Lett. 2013, 4, 722–729. (9) Zhou, Y.; Eck, M.; Veit, C.; Zimmermann, B.; Rauscher, F.; Niyamakom, P.; Yilmaz, S.; Dumsch, I.; Allard, S.; Scherf, U.; Kruger, M. Efficiency Enhancement for Bulk-Heterojunction Hybrid Solar Cells Based on Acid Treated CdSe Quantum Dots and Low Bandgap Polymer PCPDTBT. Sol. Energy Mater. Sol. Cells 2011, 95, 1232– 1237. (10) Klem, E. J. D.; Gregory, C. W.; Cunningham, G. B.; Hall, S.; Temple, D. S.; Lewis, J. S. Planar PbS Quantum Dot/C60 Heterojunction Photovoltaic Devices with 5.2% Power Conversion Efficiency. Appl. Phys. Lett. 2012, 100, 173109. (11) Tang, J.; Sargent, E. H. Infrared Colloidal Quantum Dots for Photovoltaics: Fundamentals and Recent Progress. Adv. Mater. 2011, 23,12–29. (12) Szendrei, K.; Gomulya, W.; Yarema, M.; Heiss, W.; Loi, M. A. PbS Nanocrystal Solar Cells with High Efficiency and Fill Factor. Appl. Phys. Lett. 2010, 97, 203501. (13) Choi, J. J.; Lim, Y.-F.; Santiago-Berrios, M. E. B.; Oh, M.; Hyun, B.-R.; Sun, L.; Bartnik, A. C.; Goedhart, A.; Malliaras, G. G.; Abruna, H. c. D.; Wise, F. W.; Hanrath, T. PbSe Nanocrystal Excitonic Solar Cells. Nano Lett. 2009, 9, 3749–3755. (14) Rath, A. K.; Bernechea, M.; Martinez, L.; Pelayo Garcia de Arquer, F.; Osmond, J.; Konstantatos, G. Solution-Processed Inorganic Bulk Nano-Heterojunctions and Their Application to Solar Cells. Nat. Photonics 2012, 6, 529–534. (15) Albero, J.; Zhou, Y.; Eck, M.; Rauscher, F.; Niyamakom, P.; Dumsch, I.; Allard, S.; Scherf, U.; Krueger, M.; Palomares, E. Photo Induced Charge Recombination Kinetics in Low Bandgap PCPDTBT Polymer:CdSe Quantum Dot Bulk Heterojunction Solar Cells. Chem. Sci. 2011, 2, 2396–2401. (16) Martinez-Ferrero, E.; Mora Sero, I.; Albero, J.; Gimenez, S.; Bisquert, J.; Palomares, E. Charge Transfer Kinetics in CdSe Quantum Dot Sensitized Solar Cells. Phys. Chem. Chem. Phys. 2010, 12, 2819– 2821. (17) Shalom, M.; Albero, J.; Tachan, Z.; Martinez-Ferrero, E.; Zaban, A.; Palomares, E. Quantum Dot-Dye Bilayer-Sensitized Solar Cells: Breaking the Limits Imposed by the Low Absorbance of Dye Monolayers. J. Phys. Chem. Lett. 2010, 1, 1134–1138. (18) Zewdu, T.; Clifford, J. N.; Hernandez, J. P.; Palomares, E. Photo-Induced Charge Transfer Dynamics in Efficient TiO2/CdS/ CdSe Sensitized Solar Cells. Energy Environ. Sci. 2011, 4, 4633–4638. (19) Shuttle, C. G.;

Hamilton, R.; O'Regan, B. C.; Nelson, J.; Durrant, J. R. Charge-Density-Based Analysis of the Current–voltage Response of Polythiophene/Fullerene Photovoltaic Devices. Proc. Natl. Acad. Sci. U.S.A. 2010, 107, 16448–16452. (20) Credgington, D.; Kim, Y.; Labram, J.; Anthopoulos, T. D.; Durrant, J. R. Analysis of Recombination Losses in a Pentacene/C60 Organic Bilayer Solar Cell. J. Phys. Chem. Lett. 2011, 2, 2759–2763. (21) Koster, L. J. A.; Mihailetchi, V. D.; Xie, H.; Blom, P. W. M. Origin of the Light Intensity Dependence of the Short-Circuit Current of Polymer/Fullerene Solar Cells. Appl. Phys. Lett. 2005, 87, 203502. (22) Berkel, C. v.; Powell, M. J.; Franklin, A. R.; French, I. D. Quality Factor in a-Si:H nip and pin Diodes. J. Appl. Phys. 1993, 73, 5264– 5268. (23) Zhao, N.; Osedach, T. P.; Chang, L.-Y.; Geyer, S. M.; Wanger, D.; Binda, M. T.; Arango, A. C.; Bawendi, M. G.; Bulovic, V. Colloidal PbS Quantum Dot Solar Cells with High Fill Factor. ACS Nano 2010, 4, 3743–3752. (24) Dibb, G. F. A.; Kirchartz, T.; Credgington, D.; Durrant, J. R.; Nelson, J. Analysis of the Relationship between Linearity of Corrected Photocurrent and the Order of Recombination in Organic Solar Cells. J. Phys. Chem. Lett. 2011, 2, 2407–2411. (25) Sanchez-Díaz, A.; Burtone, L.; Riede, M.; Palomares, E. Measurements of Efficiency Losses in Blend and Bilayer-Type Zinc Phthalocyanine/C60 High-Vacuum-Processed Organic Solar Cells. J. Phys. Chem. C 2012, 116, 16384–16390. (26) Maurano, A.; Shuttle, C. G.; Hamilton, R.; Ballantyne, A. M.; Nelson, J.; Zhang, W.; Heeney, M.; Durrant, J. R. Transient Optoelectronic Analysis of Charge Carrier Losses in a Selenophene/ Fullerene Blend Solar Cell. J. Phys. Chem. C 2011, 115, 5947–5957. (27) Foertig, A.; Wagenpfahl, A.; Gerbich, T.; Cheyns, D.; Dyakonov, V.; Deibel, C. Nongeminate Recombination in Planar and Bulk Heterojunction Organic Solar Cells. Adv. Energy Mater. 2012, 2, 1483–1489. (28) Bisquert, J.; Garcia-Belmonte, G. On Voltage, Photovoltage, and Photocurrent in Bulk Heterojunction Organic Solar Cells. J. Phys. Chem. Lett. 2011, 2, 1950–1964. (29) Maurano, A.; Hamilton, R.; Shuttle, C. G.; Ballantyne, A. M.; Nelson, J.; O'Regan, B.; Zhang, W.; McCulloch, I.; Azimi, H.; Morana, M.; Brabec, C. J.; Durrant, J. R. Recombination Dynamics as a Key Determinant of Open Circuit Voltage in Organic Bulk Heterojunction Solar Cells: A Comparison of Four Different Donor Polymers. Adv. Mater. 2010, 22, 4987–4992. (30) Shuttle, C. G.; O'Regan, B.; Ballantyne, A. M.; Nelson, J.; Bradley, D. D. C.; Durrant, J. R. Bimolecular Recombination Losses in Polythiophene: Fullerene Solar Cells. Phys. Rev. B: Condens. Matter Mater. Phys. 2008, 78, 113201. (31) Kirchartz, T.; Nelson, J. Meaning of Reaction Orders in Polymer:Fullerene Solar Cells. Phys. Rev. B: Condens. Matter Mater. Phys. 2012, 86, 165201. (32) Credgington, D.; Durrant, J. R. Insights from Transient Optoelectronic Analyses on the Open-Circuit Voltage of Organic Solar Cells. J. Phys. Chem. Lett. 2012, 3, 1465–1478. (33) Tang, J.; Brzozowski, L.; Barkhouse, D. A. R.; Wang, X.; Debnath, R.; Wolowiec, R.; Palmiano, E.; Levina, L.; Pattantyus Abraham, A. G.; Jamakosmanovic, D.; Sargent, E. H. Quantum Dot Photovoltaics in the Extreme Quantum Confinement Regime: The Surface-Chemical Origins of Exceptional Air- and Light-Stability. ACS Nano 2010, 4, 869–878